Optical Fiber Technology, **7**, 236–253 (2001)
doi:10.1006/ofte.2001.0358, available online at http://www.idealibrary.com on IDEAL®

An Improved All-Fiber Cross-Connect Node for Future Optical Transport Networks

Edward Mutafungwa

Communications Laboratory, Helsinki University of Technology, PL 2300 (Otakaari 8), FIN-02015 HUT, Finland

In this paper, we briefly review the current state-of-the-art in fiber devices for communication systems and propose some modifications to a previously reported all-fiber optical cross-connect node. These modifications seek to improve the node's spectral characteristics, modularity, and optical spectral efficiency. Similar recommendations are also made for optical add–drop multiplexers to be used in optical ring topologies. Using the added features, the transmission performance of the modified 2×2 node is analyzed and comparisons are made with the previously reported nodes of the same dimensions. The results indicate a significant improvement in node cascadability performance over the latter case. Further comparisons were carried out to include other types of all-fiber cross-connect nodes, with the modified node again proving to be an overall competitive solution. © 2001 Academic Press

1. INTRODUCTION

Future optical transport networks are expected to provide a format-independent (transparent) aggregation, routing, and management of signals with distinct center frequencies (wavelengths) [1]. This transparent optical networking increases the utilization of fiber capacity using wavelength division multiplexing (WDM) and provides improved flexibility for the network operator. One of the most essential enabling technologies for optical networking is the optical cross-connect node (OXN) [1], [2, chap. 8], whose primary function is to cross-connect the constituents of an aggregate WDM signal between any given set of interconnected fiber links. Moreover, this wavelength reconfiguration capability facilitates provision of bandwidth on demand, bandwidth trading, and alleviation of network congestion and makes allowances for nondisruptive expansion of the physical topology of the network. Additionally, wavelength-level management is possible for monitoring the

1068-5200/00 $35.00

integrity of existing connections and the rapid restoration of services in the event of a failure(s) within the network.

A multitude of OXNs implemented using technologies as diverse as planar lightwave circuits and bulk-optics has been reported (see [3, 4, and references quoted therein]). The inevitable need to carry out postdeployment scaling of OXN sizes due to the increase in demand for extra bandwidth (met by adding wavelength channels or lighting up dark fibers) has raised interest in simplified OXN architectures that maintain the same levels of transmission performance regardless of such size fluctuations. Fiber-based devices have been identified as one of the most promising components for implementing OXNs by virtue of their low loss, polarization independence, ease of coupling, wide operating bandwidths, robustness, and high stability. Furthermore, they have potential for volume production due to their simple and inexpensive fabrication and packaging procedures.

In this paper, we propose an improved all-fiber wavelength selective OXN suitable for future optical transport networks. The fiber devices applicable for OXN design are reviewed briefly in Section 2. Various all-fiber OXNs are introduced in Section 3 and proposals are made for performance improvement of a selected study OXN. Section 4 describes some analysis and comparisons made between the modified OXN and other previously proposed all-fiber OXNs.

2. BUILDING BLOCKS

A typical OXN consists of three main subsystems: a wavelength demultiplexer for decomposing an aggregate WDM signal into tributaries with distinct wavelengths, a switching subsystem for directing uniwavelength signals to a specified output, and a multiplexer for recombining signals of differing wavelengths onto a single fiber port prior to WDM transmission over an outgoing fiber link. Optical amplifiers may be placed on the incoming or outgoing fiber ports to boost WDM signal power in wide area networks. The node of Fig. 1 is an example of a typical OXN with a 2×2 dimension used in a 2-channel WDM system with rates of 2.5 Gb/s per channel or higher (signals with lower line rates are handled by logical switching nodes such as SDH/SONET digital cross-connects).

Recently, there has been a significant development of fiber-based devices capable of implementing the aforementioned OXN subsystems. Their architectures and suitability for optical networking applications are reviewed in the remainder of this section.

2.1. *All-Fiber (De)multiplexers*

An N wavelength demultiplexer (DMUX) is typically implemented using a $1 \times N$ passive splitting and 1 wavelength filter on each DMUX arm as illustrated in Fig. 2. Fiber Bragg gratings (FBGs), that filter signals using index perturbations written on photosensitive fibers are currently the most ubiquitous fiber filter in communication systems [5]. If perturbations are spaced at a period of Λ_g along an FBG of length L, the power of a forward-propagating wave with a center frequency λ_R is coupled

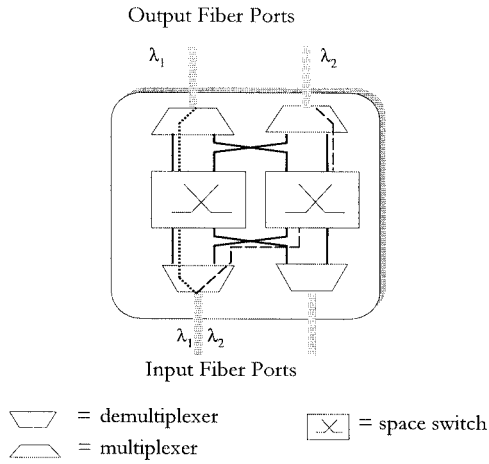

FIG. 1. A 2×2 OXN cross-connecting channels λ_1 and λ_2 along two distinct paths (dotted and dashed lines, respectively) to their predetermined output fibers ports.

to its back-propagating mode of the wave. For a given effective index n_{eff} of the guided mode of interest, by coupled mode theory the reflected wavelength of the reflection peaks is given by $\lambda_R = 2n_{eff}\Lambda_g$ [6].

An FBG is usually in the form of multiple-FBG structures or is combined with other components when performing wavelength filtering in DMUXs. For instance, the filter of Fig. 3a uses a cascade of $N - 1$ bandstop FBGs for an N-channel WDM system. Since a large N results in a chain of N FBGs written on a common fiber and having high end-to-end losses, an alternative design using only two wideband FBGs can be used to suppress channels on either side of the desired channel (see Fig. 3b [7]). However, the reflection band of practical FBGs is limited to about 10 nm [8], making this filtering arrangement unsuitable for current systems that have up to 80 nm of transmission bandwidth (erbium C- and L-bands) at their disposal [1]. This is also a limiting factor when stand-alone phase-shifted FBGs are used in Fig. 3c since their passbands are confined within the reflection band of a single FBG [9]. A filter made by writing gratings on fiber Michelson interferometers (see Fig. 3d) was proposed by Bilodeau *et al.* [10], which pro-

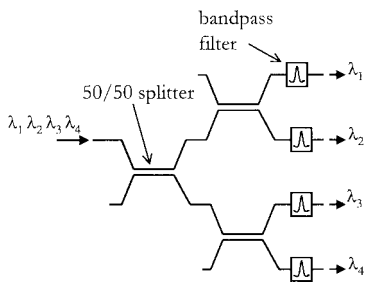

FIG. 2. Schematic of a 4-channel wavelength demultiplexer.

vides narrower passbands compared to plain FBGs, but has poor crosstalk isolation ($X = 20$ dB for 100 GHz spacing). Alternative fiber interferometer filtering configurations, namely the Sagnac loops [11] or Mach–Zehnder interferometers (MZI) [12] also fall short of the crosstalk isolation requirements ($X \geq 30$ dB) for the current generation of dense WDM systems [13]. Kewitsch *et al.* [14] propose an asymmetric or null coupling filter with an FBG inscribed on its waist as illustrated in Fig. 3e. In this case, the coupling only occurs when an acoustic wave is applied on the filter. The observed performance of the asymmetric coupling filter [14], a narrow reflection band, high crosstalk isolation ($X > 30$ dB), and low insertion loss (0.1 dB) are the best of all the fiber filters described in this section.

An all-fiber multiplexer (MUX) can be implemented using passive $N \times 1$ combiners followed by an optional filtering stage based on one of the filtering methods mentioned above.

2.2. *All-Fiber Switches*

The development of all-fiber switching lags behind the more established electro-optic, opto-mechanical, and thermo-optic switching technologies. Earlier proposals for fiber switching elements based on the 2×2 fiber MZI and a therm-optic phase-shifter (see Fig. 4a) could only guarantee a 15 dB crosstalk isolation, with a drive power requirement of 20 mW and a switching speed of just 40 ms for a switch for a 4×4 composite switch [15]. Switches using the previously described asymmetric couplers (see Fig. 4b) are relatively faster (<100 μs) and require less drive power (1 mW), but provide an insignificant increase in isolation ($X = 20$ dB) [16]. Latching-type fiber switches that use compact and low power micromachining techniques depicted in Fig. 4c promise several improvements [17]. These include (for a 1×2 switching element) negligible losses (0.36 dB), low drive-power

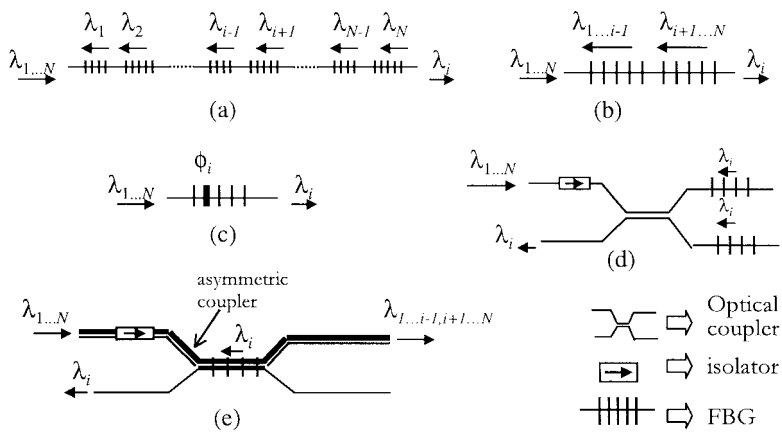

FIG. 3. Optical fiber filters implemented using (a) a chain FBGs, (b) wideband rejection FBG, (c) phase-shifted FBGs, (d) a fiber Michelson interferometer configuration, and (e) acoustically-driven asymmetric couplers.

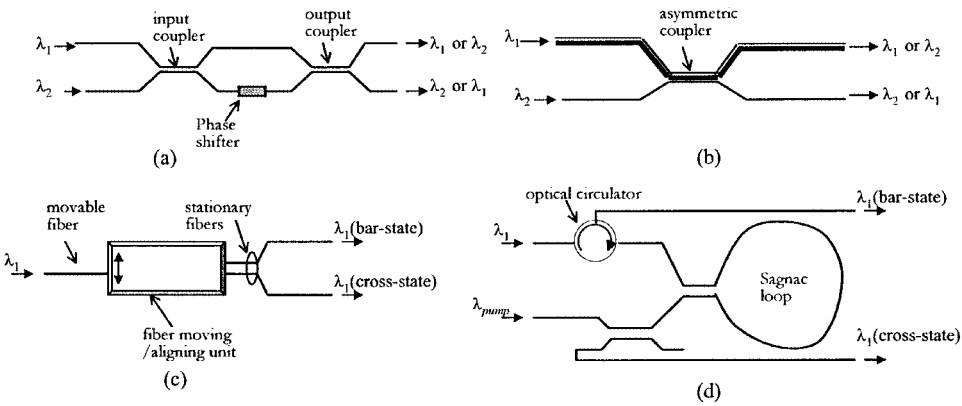

FIG. 4. All-fiber 2×2 switching using (a) a Mach–Zehnder interferometer, (b) an asymmetric coupler and 1×2 using (c) fibers-micromachining and (d) a nonlinear optical loop mirror.

(9 mW), fast switching times [26] (2 ms), and, more important, a high crosstalk isolation ($X = 70$ dB) [17]. Ultrafast switching speeds (≤ 5 μs) needed for photonic packet switching can be achieved using a pump signal and a doped nonlinear fiber for the phase-shifting operation in Fig. 4a [18]. A configuration that offers more stability for ultrafast switches is the nonlinear optical loop mirror that is based on the Sagnac interferometer [18]. This comes at a cost of the increased number of components required to realize a single 1×2 switching element, as shown in Fig. 4d.

The potential of FBGs for wavelength switching applications has also recently been recognized [5]. This stems from the fact that the Bragg wavelength λ_R can be tuned by varying the FBG's n_{eff} and Λ_g using external (stress, strain, or bending) forces and/or temperature changes that induce elongation and photoelastic effects. The resultant wavelength displacement can be expressed as [19]

$$d\lambda_R = \left[2\Lambda_{g,0}\left(\frac{\partial n_{eff}}{\partial F}\right) + 2n_{eff,0}\left(\frac{\partial \Lambda_g}{\partial F}\right)\right]dF + \left[2\Lambda_{g,0}\left(\frac{\partial n_{eff}}{\partial T}\right) + 2n_{eff,0}\left(\frac{\partial \Lambda_g}{\partial T}\right)\right]dT, \quad (1)$$

where T is the temperature, F is the applied force with $n_{eff,0}$ and $\Lambda_{g,0}$ being the FBG's initial effective refractive index and grating period, respectively. Assuming that the FBG is **ON** when $dT = dF = 0$ and is **OFF** otherwise, by using this wavelength tunable reflectivity it is possible to employ FBGs to duplicate various wavelength switching configurations.

TABLE 1
Previously Reported All-Fiber and Hybrid OXNs

OXN type	Main internal module(s)	Reference
All-fiber	FBG and 3-port optical circulators (OC)	Chen [20]
All-fiber	FBG and multiport optical circulators (MOC)	Wu [21]
All-fiber	FBG and passive optical couplers (POC)	Kim [22]
Hybrid	FBG and array waveguide gratings (AWG)	Kim [23]
All-fiber	FBG, OC, and POC	Hjelme & Storoy [24]
Hybrid	FBG, OC, and optical space switches (OSW)	Chen [20], Liaw [25]
All-fiber	FBG, polarization beam splitters (PBS), and $\frac{1}{4}$-wave plates (QWP)	Park [26]

3. ALL-FIBER OXN ARCHITECTURES

The various reported OXNs that are based on (or are dominated by) fiber components are listed in Table 1. These OXNs differ according to their various operational characteristics such as blocking properties (strictly nonblocking, rearrangably nonblocking, or blocking), routing strategy (wavelength or virtual wavelength path routing), inherent modularity (ability to scale number of in- or outgoing links and/or wavelengths without replacing any existing internal OXN modules), device technology (micro-optics, fiber-optics, integrated-optics), or architectural configuration [4]. Interestingly, the use of FBGs has meant that a majority of these OXNs are not restricted to the traditional demultiplexer-switch-multiplexer configuration of Fig. 1 that is widely used by non-fiber-based OXNs [3]. The implications of this architectural difference will be revisited throughout the remainder of this paper.

After some preliminary analysis of the OXNs in Table 1, the OXN reported by Hjelme and Storoy [24] was nominated for further study. The factors that influenced that decision includes the lack of the need for a potentially lossy DMUX stage and its elegant modularity and exclusive use of fiber devices (see Fig. 5). We propose some modifications to this study OXN that will further enhance its spectral response, optical bandwidth utilization, and modularity.

3.1. *OXN Spectral Response*

The presence of nonideal filtering modules in a cascade of OXNs encountered on a signal's path induce performance degrading effects such as intrusive crosstalk and noise components as well as narrowing of the filtering bandwidth. To improve the filtering performance of the OXN of Fig. 5, a fiber Fabry–Perot (FFP) filtering stage is added at the output of the wavelength routing unit (WRU) as shown in Fig. 6. This reduces the level of crosstalk accompanying the cross-connected signal and sharpens the precision of channel selectivity to the MHz regime. The FFP considered here is of a double-cavity Vernier-tunable ultraselective design with

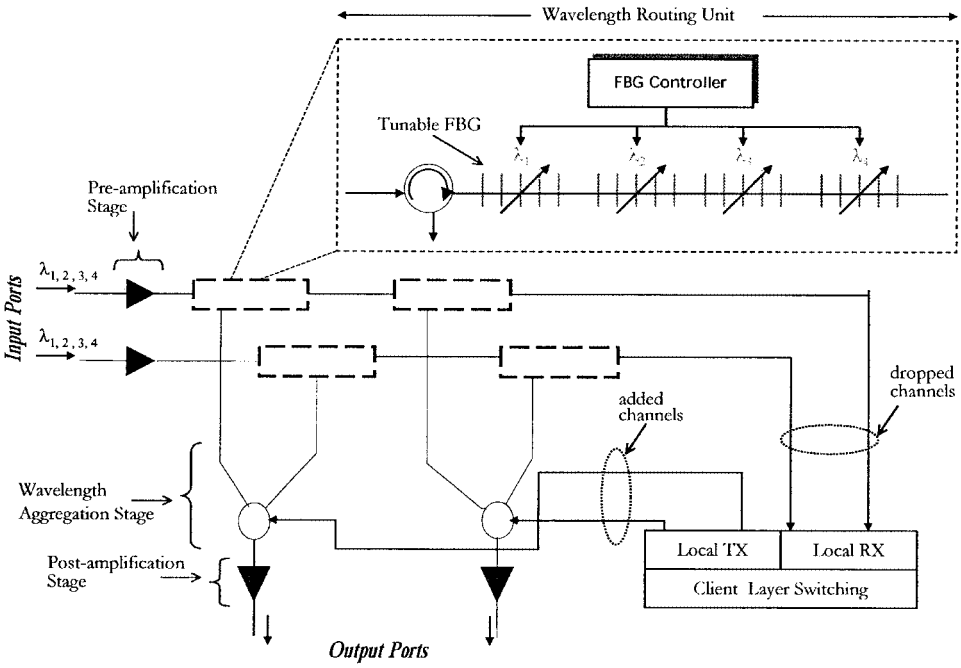

FIG. 5. OXN implemented using FBGs, circulators, and passive combiners [24].

transmission peaks that can be set by adjusting the free spectral range (FSR) of the two filtering stages. This provides an isolation that is an order of magnitude higher than single-cavity FFP filters [27] and adds more flexible wavelength tunability to the **ON–OFF** FBG tuning already available in the WRU. This dual tuning arrangement enables the OXN to cross-connect any arbitrary set of channels from an ITU (International Telecommunications Union) recommended frequency grid.

By incorporating appropriate constraints in the routing and wavelength assignment (RWA) algorithms, it is possible to obtain satisfactory transmission performance using easily fabricable uniform FBGs in the WRU. For an N-channel system, each with a nonnegative integer valued index k, if

$$Z_{ij}^{k} = \begin{cases} 1, & \text{if signal with wavelength } \lambda_k \text{ traverses} \\ & \text{link between OXNs } i \text{ and } j \\ 0, & \text{otherwise, } \forall k \in [1, N] \end{cases}$$

the constraint

$$\sum_{l=-\Gamma}^{\Gamma} Z_{ij}^{k+l} \leq 1, \qquad i \neq j, \tag{2}$$

lowers the crosstalk penalties by increasing Γ. This ensures that the members of channel set

$$\{\Gamma \in [2, N[: \lambda_{k-\Gamma}, \ldots, \lambda_{k-1}, \lambda_k, \lambda_{k+1}, \ldots, \lambda_{k+\Gamma}\} \tag{3}$$

cannot share the same OXN output port or have a common fiber link in their paths. In this case the combined transmittance of the WRU is [8, 28]

$$T(f) = |H_1|^2 \cdot |H_2|^2 \cdot \frac{\sinh^2(L\sqrt{\kappa^2 - \hat{\sigma}_f})}{\cosh^2(L\sqrt{\kappa^2 - \hat{\sigma}_f}) - \frac{\hat{\sigma}_f}{\kappa^2}}, \tag{4}$$

where the transfer function of the ith FFP filter stage with a filter reflection coefficient R is

$$H_i(f) = \frac{1 - R}{1 - R \cdot e^{j2\pi \frac{f}{FSR_i}}}, \tag{5}$$

and from (4) κ and $\hat{\sigma}_f$ are the respective AC and period-averaged coupling coefficients of an L long FBG. We illustrate this with an example of an WRU for an 8-channel system spaced at $\Delta f = 100$ GHz, with $\lambda_{3,7}$ being the dropped channels ($\Gamma = 3$) and $\text{FSR}_i = \Delta f, i \in \{1, 2\}$. The spectral response of the **ON** FBGs and FFP in the WRU is depicted in Fig. 7. The worst-case level of crosstalk leaked is about 30 dB and is located 200 GHz from either channel.

Alternatively, the use of more complex optimized apodized FBGs can relax the wavelength assignment constraint introduced above. This improves the reuse of limited wavelength resources since adjacent channels on same path are packed more closely. This is possible because, unlike uniform FBGs, apodized FBGs have a dc-averaged Gaussian index varying profile that offers higher sidelobe suppression (offering an extra 20 dB suppression for $\Delta f = 100$ GHz [29]) and a flat passband.

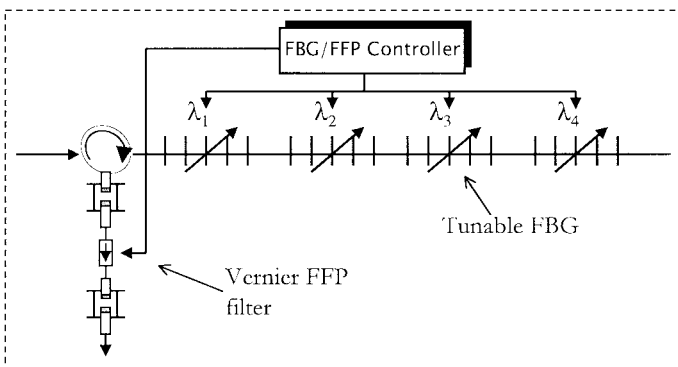

FIG. 6. A WRU enhanced by the addition of a Vernier FFP filter.

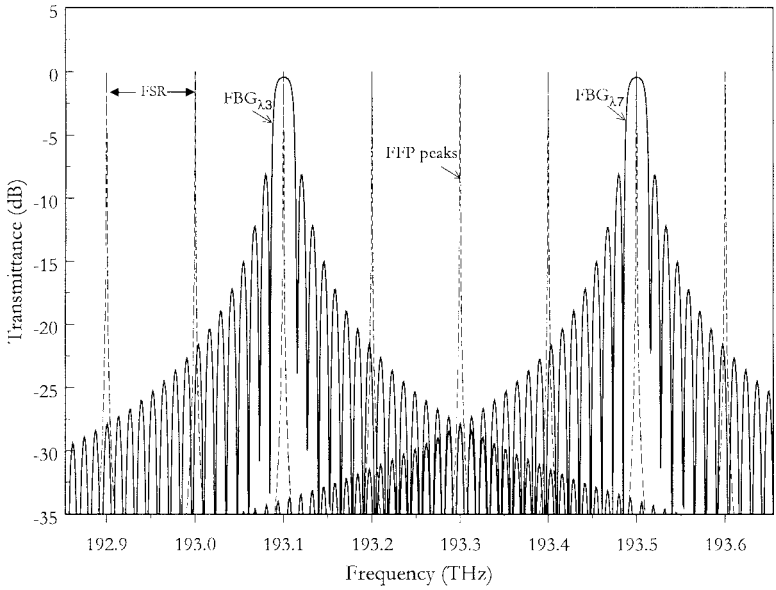

FIG. 7. Spectral responses of two uniform gratings with $\lambda_R = 1552.52$ nm (193.1 THz) and 1549.32 nm (193.5 THz) (solid line) and a Vernier FFP filter with $FFP_{1,2} = 100$ GHz (dashed line).

3.2. *Optical Bandwidth Utilization*

The utilization of the optical transmission bandwidth of an N-channel system can be quantified by the optical spectral efficiency $\eta_0 = NB_r/\Delta f$ (bit/s/Hz), where B_r is the common line rate. Due to the possibility of interferometric crosstalk, frequency drift of optical sources, and imperfect receiver or filter tuning, there is a lower bound on Δf. Another factor that is likely to limit the minimum spacing, is unique to OXNs considered here, that use FBGs in their switching subsystems. For instance, an FBG with a Bragg wavelength λ_k (that is the channel it reflects when in the **ON** state) will reflect a signal with a wavelength $\lambda_k + \Delta\lambda_k$ in its **OFF** state determined by the expression (1). It is obvious that $\Delta\lambda$ (Δf in wavelength units) has to be large enough to avoid any overlap between the reflection spectrum of an **OFF** FBG and the copropagating adjacent channel $\lambda_{k+1} \equiv \lambda_k + \Delta\lambda$ that might be fortuitously reflected or attenuated.

A rather straightforward solution to this problem would be to ensure that $\lambda_k + \Delta\lambda_{R,k}$ lies outside the 1530–1610 nm transmission window used by amplified WDM systems. This implies that $\Delta\lambda_{R,k}$ should be at least 80 nm to eliminate any possibility of overlap with the adjacent channel. A wavelength shift that is unattainable using silica FBGs. The strain-tuning of FBGs using magnetic-actuation and compressive piezoelectric transducers (PZT) can only achieve wavelength shifts of 15.7 [30] and 45 nm [31], respectively. Since the FBGs have a temperature coefficient of only 1 nm/100 °C [31], thermal tuning is also unlikely to offer any significant reflection wavelength shift values. Recently FBGs have been written on plastic or polymer fibers, producing polymer Bragg gratings (PBGs) that promise higher wavelength shifts. Translation of Bragg wavelengths by thermally-tuned pla-

nar PBGs has reached 20 nm as a result of their temperature coefficients being 25 times lower than silica FBGs [32]. Moreover, strain-tuned polymethylmethacrylate (PMMA) cladded fiber PBGs have demonstrated the wavelength shifts ($\Delta\lambda_R \geq$ 80 nm) useful for WRU, since polymer fibers possess strain recovery flexibility (essential for wavelength tuning repeatability) that is significantly higher than silica fibers [33]. Other potential advantages of using PBGs include their low cost, tolerance to adverse environmental conditions, and back-compatibility since they can be fabricated by conventional phase mask fabrication techniques used to produce silica FBGs [6].

3.3. *Improved Modularity*

Initial sizes of deployed modular OXNs are just large enough to handle short-term traffic estimates of a given service area. Thus the network operator is able to minimize the installed-first costs by avoiding unnecessary overbuilding and to only add modules in the OXN subsystems when the demand for extra bandwidth arises. The modularity of such OXNs can be classified according to the ease in which new fiber links (link modularity or L-Mod) or wavelengths (wavelength modularity or λ-Mod) can be added without sacrificing any existing OXN components [4]. Unfortunately, the increase in OXN size further accentuates the detrimental effects of module imperfections on the signals they handle [13]. Furthermore, there is an expected deterioration in node dependability (availability performance and its influencing factors) and increased running costs that limits the potential returns on the investment of added OXN components [34]. Additional concerns for the study OXN arise due to the fact that an increase in wavelength numbers implies a lengthening of the FBG cascade in the WRU. The consequence of this is the gradual narrowing of the filter bandwidth and the successive dispersion of nonreflected channels due to the out-of-band dispersive properties of FBGs [35].

Optical (or wavelength) granularity has been proposed to reduce the rate at which an OXN grows with increased bandwidth [36]. The essence of this technique is that the demand between each node pair is pre-assigned wavelength bands with G adjacent wavelength slots, thus enabling them to be routed as a group instead of as individual wavelength channels. A major advantage of this is that the number of devices in some stage of the OXN can be reduced by a factor G. The spectral resource allocation plots of Fig. 8 illustrate the assignment of wavelength channels between a source node A and destination nodes B, C, and D for systems with(out) optical granularity. When no optical granularity is used (Fig. 8 (top)), the increase in bandwidth demand between OXNs A and B or D is accommodated by assigning the next free channel on the whole wavelength set while if optical granularity with $G = 3$ is used (Fig. 8 (bottom)), new channels are only selected from the idle channels in the pre-assigned wavelength band of the particular demand pair.

The architectural implications of optical granularity on the study of OXN is that only $\lfloor N/G \rfloor$ is a ceiling function that rounds toward $+\infty$) tunable FBGs are needed, with each simultaneously reflecting G closely packed signals (see the modified WRU of Fig. 9). The limit of the FBG reflection bandwidth will place an upper bound on

G (for example, up to 13 channels with 100 GHz spacing can be placed in a 10 nm window).

3.4. *Optical Add–Drop Multiplexers*

The anticipated evolution from current point-to-point WDM links to WDM ring topologies will be supported by the deployment of optical add-drop multiplexers (OADMs) [3]. Since an OADM is a special case of an OXN with a node degree of 1 (single input–output fiber), the improvements recommended in this section are equally applicable to all-fiber OADMs. The revised OADM architecture of Fig. 10 benefits from improvements in spectral response and efficiency, dependability, and reduced complexity. The results of such ameliorations enables the construction of unidirectional single fiber rings with large diameter (reach) or alternatively a large number of interconnected rings with little or no electronic regeneration required for the longest signal paths.

Other possible optical ring implementations can make use of the modified 2×2 OXN for constructing two or four fiber bidirectional shared protection ring (SPRING) architectures [2, chap. 10]. Each input fiber port is then assigned to cater for either the clockwise or the counterclockwise working fibers. In the event of failure in a working, additional 2×2 fiber switches placed at each OXN input port may be used to switch from the working to the protection fiber (if a four fiber SPRING is used).

4. PERFORMANCE COMPARISON

A comparison of the performance of various all-fiber (or hybrid fiber) OXNs is presented in this section.

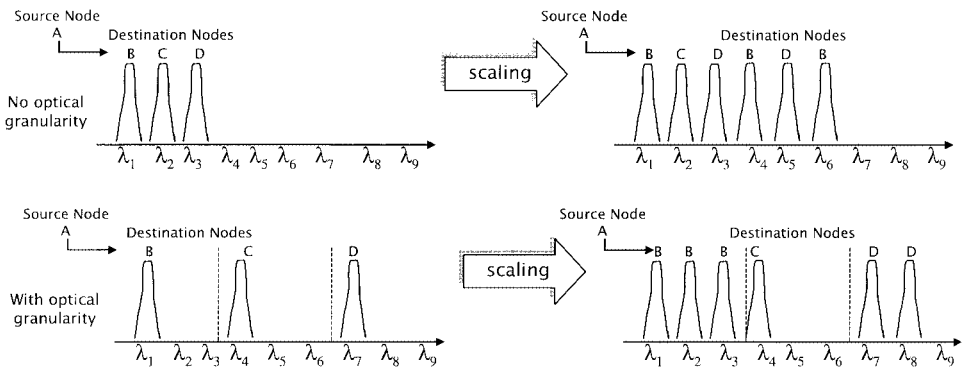

FIG. 8. Wavelength resource allocation schemes for call requests between source node A and destination nodes B, C, and D.

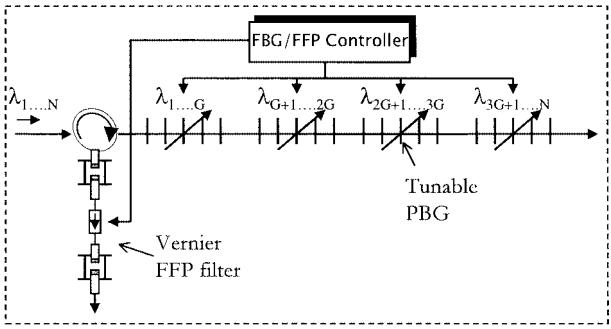

FIG. 9. A WRU modified for optical granularity (G banded signals).

4.1. *Transmission Performance*

Modeling of the transmission performance of OXNs is carried out using Photonic Transmission Design Suite (PTDS version 1.3), a wavelength-domain simulator running on a Windows NT platform [37]. A 4-channel WDM system using the intensity modulated–direct detection (IM/DD) scheme is assumed; the bit rate per channel is set at 2.5 Gbit/s ($2^7 - 1$ PRBS). The channels are spaced at 100 GHz and the emission frequencies of the transmitters range from 192.95 to 193.25 THz. The externally modulated transmitters have an extinction ratio of 30 dB with the maximum power per channel being 1 mW.

The simulation configuration is based on an optical circulating loop consisting of a 2×2 OXN under test, a single-mode (G.652) fiber link, and a spool of dispersion compensating (G.653) resulting in a total loop length of 35 km. The OXN is preceded by a pre-amplifier and is followed by an automatic gain-controlled boost amplifier to compensate for the insertion losses of OXN subsystems. By configuring the OXN to cross-connect the paths of $\{\lambda_1, \lambda_3\}$ from an incoming fiber port to diagonally located output fiber and retaining signals $\{\lambda_2, \lambda_4\}$ on their correspond-

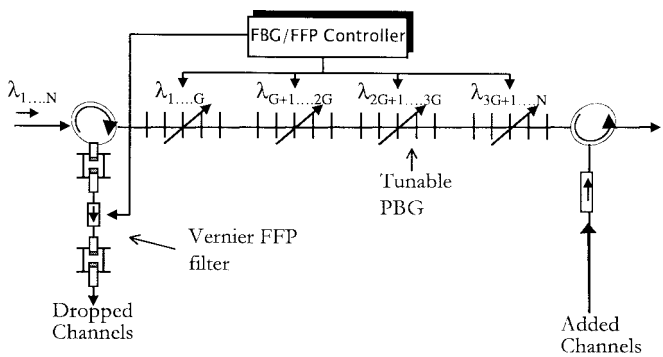

FIG. 10. An OADM that has adapted the improvements proposed for the studied OXN.

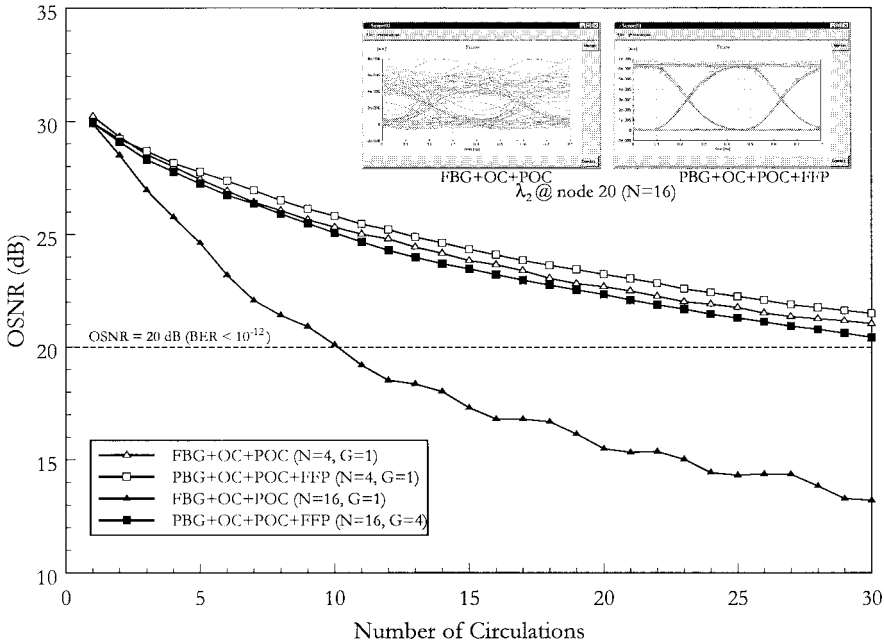

FIG. 11. Comparison of the OSNR variation with node number for study and modified OXNs. The eye diagrams for λ_2 at the 20th OXN are shown inset.

ing output fiber ports, the latter signals are able to traverse all the intermediate nodes (equivalent to the number of recirculation loop cycles). This facilitates the assessment of node cascadability by carrying out the performance analysis of either one of these 2 channels at the destination node.

The optical signal to noise ratio (OSNR) performance of λ_2 for up to 30 circulations (30 OXNs and 1050 km of fiber) is shown in Fig. 11. If the signal quality acceptance level is set at OSNR $\geq$ 20 dB to maintain a bit error rate (BER) of less than 10^{-12} [2], up to 30 OXNs can be traversed for both of the OXNs considered. However, if the number of channels is now increased to 16 (quadrupling the number of FBGs required), only 10 OXNs are cascadable using the study OXN (FBG + OC + POC) whilst the modified OXN maintains the 30 node reach. The modified OXN (PBG + OC + POC + FFP) exhibits relatively lower deterioration in signal quality because the use of optical granularity ($G = 4$) enables it to handle the added channels without the need for extra PBGs. The received eye diagrams the λ_2 signal received at the 20th node is shown in the inset of Fig. 11 indicating the severe distortion incurred by using the study OXN (**left**) with more severe dispersion by FBGs and a higher number of crosstalk interferers.

4.2. *Other Attributes*

Additional OXN attributes that determine not only the extent of node induced degradation of signal quality but other limiting effects (e.g., OXN latency, com-

TABLE 2
Performance Comparison of Various Proposed Fiber-Based OXNs (the Modified OXN Is Listed on the Final Row)

OXN	λ-Mod	L-Mod	Bidirectional	$X_{\min}$ ($\Delta f = 50$ GHz) (dB)	Ψ (N)
FBG + M(OC)	Full	Full	No	30	$N+2$
FBG + POC	Full	Full	Yes	30	$N+2$
FBG + AWG	Limited	None	No	<30	5
FBG + OC + POC	Full	Full	No	30	$N+2$
FBG + OC + OSW	Full	Limited	No	30	$2N+3$
FBG + PBS + QWP	Limited	None	Yes	25	$N+4$
PBG + OC + POC + FFP	Full	Full	No	>30	$\lfloor N/G \rfloor + 3$

plexity, flexibility) need to be considered. These are shown in Table 2, with the respective performance level of the OXNs described for each attribute. The architectural configuration of the OXN has a significant influence on its modularity. This is notable for the OXNs based on AWG and PBS whose dimension cannot be scaled beyond 2×2, thus restricting their use to applications such as ring interconnection. It is noted that the node presented in this paper (PBG + OC + POC + FFP) offers favorable advantages on all attributes except for its apparent lack of bidirectional operation. This drawback can be overlooked, since most proposals for bidirectional OXNs do not demonstrate how two different routing configurations (one for each direction) can be simultaneously accommodated on a single OXN without the possibility of increased blocking in both directions.

The impact of the increase in size (internal module number) of a modular OXN has a direct bearing on the overall node induced crosstalk power penalty and a signal's power loss incurred between the input and output ports of the node. The parameter Ψ represents the maximum number of OXN modules (excluding optical amplifiers) traversed by a signal and is a function of the number of channels N per fiber. This is dependent on an OXN type and their respective configurations (see expressions for 2×2 OXNs shown in Table 2). A low Ψ means that a signal is subjected to less attenuation, distortion, and delay as it traverses an OXN. For the modified OXN, Ψ can be lowered by setting a large granularity G. The constant Ψ for the FBG + AWG is slightly misleading, since a large N produces AWGs with dimensions of $1 \times N$ and $N \times 1$. It has been noted that AWGs have loss and crosstalk characteristics that are dependant on their dimensions [38]; thus the transmission performance of the OXN using AWGs would also drop with an increase in N. Figure 11 shows the increase in module number with wavelengths for the various OXNs (since some lack L-Mod, only 2×2 OXN are considered); this can be used as a measure of an OXN's complexity. Without the use of optical granularity ($G = 1$), the module count of the modified OXN is among the highest of all the considered OXN. However, an increase of G shows a continuous reduction in device numbers (less FBGs required), the lowest overall in Fig. 11 being for the case when $G = 16$.

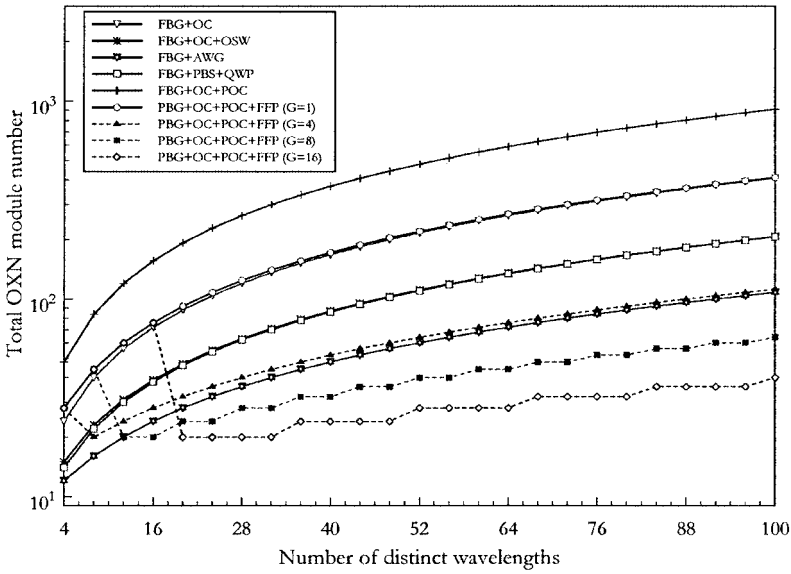

FIG. 12. Increase in total intra-OXN module number with number of distinct wavelength channels. The cases where the modified OXN uses optical granularity ($G > 1$) are indicated by dashed lines.

5. CONCLUSIONS

The modifications outlined above, when considered collectively, produce an all-fiber OXN with a transmission performance that significantly boosts its cascadability. Furthermore, we have shown that the modified OXN is highly modular, adjusting efficiently to any increase in wavelength channel number or fiber links. However, the width of the PBG's reflection band cannot be adjusted after the fabrication process, so one is restricted to the initial set values of G (unless, of course, the PBGs are replaced with gratings of different reflection bandwidths).

These recommended modifications are not restricted to the study OXN, but can also be applied on other reported all-fiber OXNs as well as OADMs. Based on the discussions and analysis presented here, we have shown that the implementation of those modifications is feasible with the currently available devices and flexible routing techniques.

APPENDIX

List of Symbols

N	Number of distinct wavelength channels
λ_R	Bragg wavelength
$\Delta\lambda_R$	Shift in Bragg wavelength
n_{eff}	Effective refractive index

L	Length of FBG
Λ_g	Effective refractive index
F	Exerted force
T	Operating temperature
λ_k	Signal with wavelength centered at channel k
κ	AC coupling coefficient
$\hat{\sigma}_f$	Period averaged coupling coefficient
R	Reflection coefficient
FSR	Free spectral range
Δf	Channel spacing
$\lambda_{R,k}$	Shift in Bragg wavelength for λ_k
η_0	Optical spectral efficiency
B_r	Line rate
G	Number of grouped adjacent wavelength channels
$OSNR$	Optical signal to noise ratio
BER	Bit error rate
Ψ	Number of modules passed by a signal in an OXN

REFERENCES

[1] H. Yoshimura, K.-I. Sato, and N. Takachio, "Future photonic transport networks based on WDM technologies," *IEEE Commun. Mag.,* vol. 37, no. 2, 74 (1999).

[2] R. Ramaswami and S. N. Kumar. *Optical Networks: A Practical Perspective,* Kaufmann, San Francisco, 1999.

[3] N. A. Jackman, S. H. Patel, B. P. Mikkelsen, and S. K. Korotky, "Optical cross-connects for optical networking," *Bell Labs Technol. J.,* vol. 4, no. 1, 246 (1999).

[4] E. Iannone and R. Sabella, "Optical path technologies: a comparison among different cross-connecting architectures," *IEEE J. Lightwave Technol.,* vol. 14, no. 10, 2184 (1996).

[5] C. R. Giles, "Lightwave applications of fiber Bragg gratings," *IEEE J. Lightwave Technol.,* vol. 15, no. 8, 1391 (1997).

[6] K. O. Hill and G. Meltz, "Fiber Bragg grating technology fundamentals and overview," *IEEE J. Lightwave Technol.,* vol. 15, no. 8, 1263 (1997).

[7] V. Mizrahi, T. Erdogan, D. J. DiGiovanni, and P. J. Lemaire, "Four channel fibre grating demultiplexer," *IEE Electron. Lett.,* vol. 30, no. 10, 730 (1994).

[8] T. Erdogan, "Fiber grating spectra," *IEEE J. Lightwave Technol.,* vol. 15, no. 8, 1277 (1997).

[9] R. Ramaswami and S. N. Radic, "Phase-Shifted Fiber Bandpass Bragg and their Application for Wavelength Demultiplexing," *IEEE Photon. Technol. Lett.,* vol. 6, no. 8, 995 (1994).

[10] F. Bilodeau, K. O. Hill, B. Malo, D. C. Johnson, and J. Albert, "Phase-shifted fiber bandpass Bragg and their application for wavelength demultiplexing," *IEEE Photon. Technol. Lett.,* vol. 6, no. 1, 80 (1994).

[11] D. P. Hand, "Single-mode filters written into Sagnac loop using photosensitive fibre: transmission filters" in *IOOC'89 Technical Digest,* vol. 4, pp. 64–65, Jul. 1989.

[12] F. Bilodeau, D. C. Johnson, S. Thériault, B. Malo, J. Albert, and K. O. Hill, "An all-fiber dense-wavelength-divison multiplexer/demultiplexer using photoimprinted Bragg gratings," *IEEE Photon. Technol. Lett.,* vol. 7, no. 4, 388 (1995).

[13] L. Gillner, C. P. Larsen, and M. Gustavsson, "Scalability of optical multiwavelength switching networks: crosstalk analysis," *IEEE J. Lightwave Technol.,* vol. 17, no. 1, 58 (1999).

[14] A. S. Kewitsch, G. A. Rakuljic, P. A. Willem, and A. Yariv, "All-fiber zero-insertion-loss add-drop filter for wavelength-division multiplexing," *Opt. Lett.,* vol. 23, no. 2, 106 (1998).

[15] A. El Fatatry, S. P. Shipley, and R. Tyson, "4 × 4 All-fiber optical switching matrix," *IEE Electron. Lett.,* vol. 24, no. 6, 339 (1988).

[16] D. O. Culverhouse, T. A. Birks, S. G. Farwell, and P. St. J. Russell, "3 × 3 All-fiber routing switch," *IEEE Photon. Technol. Lett.,* vol. 9, no. 3, 333 (1997).

[17] S. Nagaoka, "Compact latching-type single-mode-fiber switches fabricated by a fiber-micromaching technique and their practical applications," *IEEE J. Select. Topics Quantum Electron.,* vol. 5, no. 1, 36 (1999).

[18] M. J. F. Digonnet, R. W. Sadowski, H. J. Shaw, and R. H. Pantell, "Resonantly enhanced nonlinearity in doped fibers for low-power all-optical switching: a review," *Opt. Fiber Technol.,* vol. 3, no. 1, 44 (1997).

[19] R. Gafsi and M. A. El-Sherif, "Analysis of induced-birefringence effects on fiber Bragg gratings," *Opt. Fiber Technol.,* vol. 6, no. 3, 44 (2000).

[20] Y.-K. Chen and C.-C. Lee, "Fiber Bragg grating-based large nonblocking multiwavelength cross-connects," *IEEE J. Lightwave Technol.,* vol. 16, no. 10, 1746 (1998).

[21] X. Wu, Y. Shen, C. Lu, T. H. Cheng, and M. K. Rao, "Fiber Bragg grating-based rearrangable nonblocking optical cross connects using multiport optical circulators," *IEEE Photon. Technol. Lett.,* vol. 12, no. 6, 696 (2000).

[22] K.-H. Kim, S.-W. Kwon, J.-W. Park, S.-B. Lee, and S.-S. Choi, "A new all-fiber bidirectional optical cross-connect with tunable fiber Bragg gratings" in *Technical Digest of OFC'99*, San Diego, vol. 1, pp. 261–261, 1999.

[23] J. Kim, J. Jung, S. Kim, and B. Lee, "Reconfigurable optical cross-connect using WDM MUX/DEMUX pair and tunable fibre Bragg gratings," *IEE Electron. Lett.,* vol. 36, no. 1, 67 (2000).

[24] D. Hjelme and H. Storoy, "Reconfigurable all-fiber all-optical cross-connect node using synthesized fiber Bragg gratings for both demultiplexing and switching" in *Technical Digest of OFC'98,* San Jose, vol. 1, pp. 65–66, 1998.

[25] S.-K. Liaw, K.-P. Ho and S. Chi, "Multichannel add/drop and cross-connect using fibre Bragg gratings and optical switches," *IEEE Photon. Technol. Lett.,* vol. 34, no. 16, 1601 (1998).

[26] S.-K. Park, J.-W. Park, S.-R. Lee, H. Yoon, S.-B. Lee, and S.-S. Choi, "Multiwavelength bidirectional optical crossconnect using fiber Bragg gratings and polarization beam splitter," *IEEE Photon. Technol. Lett.,* vol. 10, no. 4, 531 (1998).

[27] P. Humblet and W. M. Hamdy, "Crosstalk analysis and filter optimization of single- and double-cavity Fabry-Perot filters," *IEEE J. Select. Areas Commun.,* vol. 8, no. 6, 1095 (1990).

[28] B. Ortega, J. Capmany and J. L. Cruz, "Wavelength division all-fiber fybrid devices based on Fabry-Perot's and gratings," *IEEE J. Lightwave Technol.,* vol. 17, no. 7, 1241 (1999).

[29] A. Inoue, T. Iwashama, T. Enomoto, S. Ishikawa, and H. Kanamori, "Optimization of fiber Bragg grating for dense WDM transmission system," *IEICE Trans. Electron.,* vol. E81-C, no. 8, 1209 (1998).

[30] S. Jin, H. Mavoori, R. P. Espindola, L. E. Adams, and T. A. Strasser, "Magnetically tunable fiber Bragg gratings" in *Technical Digest of OFC'99,* vol. 3, pp. 135–137, Feb. 1999.

[31] H. G. Limberger, A. Iocco, R. P. Salathé, L. A. Everall, K. E. Chisholm, and I. Bennion, "Wideband tuneable fibre Bragg grating filters," in *STeP 2000,* pp. 9–16, Aug. 2000.

[32] L. Eldada, R. Blomquist, M. Maxfield, D. Pant, G. Boudoughian, C. Poga, and R. A. Norwood, "Thermooptic planar polymer Bragg grating OADMs with broad tuning range," *IEEE Photon. Technol. Lett.,* vol. 11, no. 4, 448 (1999).

[33] Z. Xiong, G. D. Peng, B. Wu, and P. L. Chu, "Highly tunable Bragg gratings in single-mode polymer optical fibers," *IEEE Photon. Technol. Lett.,* vol. 11, no. 3, 352 (1999).

[34] E. Mutafungwa, "Application of a genetic algorithm to optical cross-connect node dependability enhancement," in *Proc. Finnish Artificial Intelligence Conf.,* Espoo, pp. 9–16, 2000.

[35] Y.-K. Chen and C.-C. Lee, "Dispersion of cascaded fiber gratings in WDM lightwave systems," *IEEE J. Lightwave Technol.,* vol. 16, no. 8, 1523 (1998).

[36] E. Ciaramella, "Introducing Wavelength Granularity to Reduce the Complexity of Optical Cross Connects," *IEEE Photon. Technol. Lett.,* vol. 12, no. 6, 699 (2000).

[37] A. Lowery, O. Lenzmann, I. Koltchanov, R. Moosburger, R. Freund, A. Richter, S. Georgi, D. Breuer, and H. Hamster, "Multiple signal respresentation simulation of photonic devices, system and networks," *IEEE J. Select. Topics Quantum Electron.,* vol. 6, no. 2, 282 (2000).

[38] A. Kaneko, A. Sugita and K. Okamoto, "Recent progress on arrayed waveguide gratings for DWDM applications," *IEICE Trans. Electron,* vol. E83-C, no. 6, 860 (2000).